Chemosphere 288 (2022) 132417

Contents lists available at ScienceDirect

Chemosphere

journal homepage: www.elsevier.com/locate/chemosphere

Experimental insights into anodic oxidation of hexafluoropropylene oxide dimer acid (GenX) on boron-doped diamond anodes

Diwakar Suresh Babu [a,**], Johannes M.C. Mol [a], Josephus G. Buijnsters [b,*]

[a] Department of Materials Science and Engineering, Delft University of Technology, Mekelweg 2, 2628 CD Delft, The Netherlands
[b] Department of Precision and Microsystems Engineering, Research Group of Micro and Nano Engineering, Delft University of Technology, Mekelweg 2, 2628 CD Delft, The Netherlands

HIGHLIGHTS

- Direct electron transfer is the rate-determining step in HFPO-DA degradation.
- $OH^{\bullet}$ generation on the boron-doped diamond anode is crucial for C–F bond cleavage.
- $SO_4^{\bullet-}$ is ineffective in HFPO-DA degradation due to steric hindrance by $–CF_3$ branch.
- $-CF_3$ branch increases complexity of direct electron transfer in HFPO-DA.
- Defluorination rate is faster for HFPO-DA than for PFOA due to lesser intermediates.

GRAPHICAL ABSTRACT

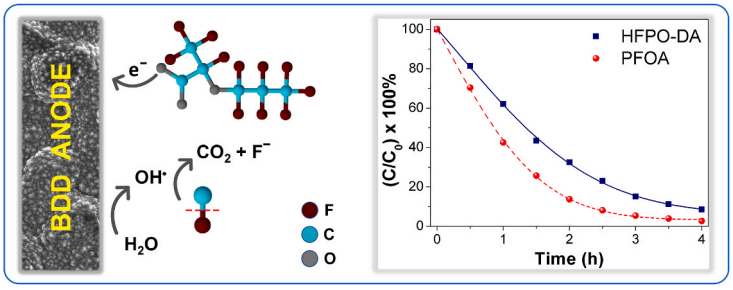

ARTICLE INFO

Handling Editor: E. Brillas

Keywords:
Boron-doped diamond (BDD)
Hexafluoropropylene oxide dimer acid (HFPO-DA)
GenX
Electrochemical oxidation
Hydroxyl radicals
Perfluorooctanoic acid (PFOA)

ABSTRACT

GenX is the trade name of the ammonium salt of hexafluoropropylene oxide dimer acid (HFPO-DA) and is used as a replacement for the banned perfluorooctanoic acid (PFOA). However, recent studies have found GenX to be more toxic than PFOA. This work deals with the electrochemical degradation of HFPO-DA using boron-doped diamond anodes. For the first time, an experimental study was conducted to investigate the influence of sulfate concentration and other operating parameters on HFPO-DA degradation. Results demonstrated that sulfate radicals were ineffective in HFPO-DA degradation due to steric hindrance by $–CF_3$ branch. Direct electron transfer was found as the rate-determining step. By comparing degradation of HFPO-DA with that of PFOA, it was observed that the steric hindrance by $–CF_3$ branch in HFPO-DA decreased the rate of electron transfer from the carboxyl head group even though its defluorination rate was faster. Conclusively, a degradation pathway is proposed in which HFPO-DA mineralizes to CO_2 and F^- via formation of three intermediates.

1. Introduction

Per- and polyfluoroalkyl substances (PFAS) are man-made substances containing at least 4730 different chemical varieties in its family (The Organisation for Economic Co-operation and Development (OECD), 2018; Goeden et al., 2019). They are made of a chain of C–F bonds which are one of the strongest bonds known (531.5 kJ mol^{-1}) (Parsons et al., 2008; Vecitis et al., 2009; Zhang et al., 2013). Since their

* Corresponding author.
** Corresponding author.
E-mail addresses: diwakar.psuresh@gmail.com (D. Suresh Babu), J.M.C.Mol@tudelft.nl (J.M.C. Mol), J.G.Buijnsters@tudelft.nl (J.G. Buijnsters).

https://doi.org/10.1016/j.chemosphere.2021.132417
Received 24 July 2021; Received in revised form 24 September 2021; Accepted 28 September 2021
Available online 1 October 2021

invention in the 1930s, PFAS have been extensively used in fire-fighting foams, non-stick cookware, textiles and food packaging materials due to their hydrophobic, oleophobic and surfactant properties (Baran, 2001; Prevedouros et al., 2006; Davis et al., 2007; McGuire et al., 2014; Niu et al., 2016). Owing to their high chemical stability, inability to degrade naturally and resistance to conventional treatment methods like flocculation, coagulation and ozonation (Rahman et al., 2014; Hopkins et al., 2018), PFAS are nicknamed as "forever chemicals" (Cheryl Hogue, 2019).

By their chemical constitution, PFAS inherently pose severe health and environmental concerns. Perfluorooctanoic acid (PFOA) and perfluorooctanesulfonate (PFOS) are the most widely studied PFAS due to their widespread contamination of various environmental and biological matrices including groundwater (Cousins et al., 2016; Hongkachok et al., 2018), surface water (Gobelius et al., 2018; Wang et al., 2019; Baabish et al., 2021), drinking water (Hu et al., 2016; Daly et al., 2018; Domingo and Nadal, 2019), sediments (Guo et al., 2010; Pico et al., 2012), human serum (Olsen et al., 2007; Fujii et al., 2017) and animal tissue (Kannan et al., 2004). A recent study showed that elevated plasma-PFAS concentration in human blood is associated with the severe course of COVID-19 due to their accumulation in lungs (Grandjean et al., 2020). Taking into account their persistent toxicity and bioaccumulation, PFOA was listed in the Annex A (elimination) and PFOS was listed in the Annex B (restriction) of the Stockholm Convention on Persistent Organic Pollutants for a global ban (Conder et al., 2008; Springer Berlin Heidelberg, 2013). Due to their phase-out, short-chain fluorinated compounds such as perfluoroalkyl ether carboxylic and sulfonic acids (PFECAs and PFESAs) are being used as alternatives (Bao et al., 2020).

Hexafluoropropylene oxide dimer acid (HFPO-DA, $C_6HF_{11}O_3$, CAS no: 13252-13-6) belongs to a class of PFECAs. The ammonium salt of HFPO-DA has the trade name GenX. Both HFPO-DA and GenX exist in the same anionic form ($C_6F_{11}O_3^-$) in water due to deprotonation (H^+) or dissociation (NH_4^+), respectively, and thus can be considered the same dissolved species. GenX is commercialized by Chemours and is currently used as a replacement of PFOA in fluoropolymer production plants (Chemours named in GenX lawsuit, 2017). However, recent studies have shown that GenX has higher toxicity compared to PFOA (Gomis et al., 2018) and is more easily soluble in water, thus making it more difficult for removal (Mullin et al., 2019). In recent years, GenX has been detected in surface water, drinking water and in tissues of fish near the production plants in Europe, China and the United States (Heydebreck et al., 2015; Sun et al., 2016; Brandsma et al., 2019). In 2019, GenX was added to the list of Substances of Very High Concern due to its potential adverse health effects (ECHA, 2020). In The Netherlands, The National Institute for Public Health and the Environment (RIVM) has set a safe limit of GenX exposure from drinking water (150 ng L^{-1}), surface water (118 ng L^{-1}) and consumption of fish (2.6 μg kg^{-1}) (Beekman et al., 2016; RIVM, 2019). Production of these short-chain fluorinated alternatives, however, still continues because of their unique repellant properties that are not easily achievable by non-fluorinated compounds (Bao et al., 2020).

Advanced treatment approaches like nanofiltration and reverse osmosis have shown effective removal efficiency (Appleman et al., 2013; Flores et al., 2013; Soriano et al., 2017; Boo et al., 2018; Banks et al., 2020), but the disposal of the concentrated PFAS retentate is still a problem (Lang et al., 2017; Stoiber et al., 2020). On the other hand, electrochemical advanced oxidation processes (EAOPs) are one of the most studied methods for PFAS degradation due to the generation of highly reactive hydroxyl radicals ($OH^•$) with a high redox potential (E° = 2.8 V vs SHE) (Moreira et al., 2017; Amor et al., 2019) and their potential to cleave the highly stable C–F bonds through formation of thermally unstable alcohol compound (Niu et al., 2013). Among EAOPs, anodic oxidation is a widely used technique due to its effectiveness and ease of set-up in existing water treatment plants. The anodic material plays an important role in determining the degradation efficiency and materials like boron-doped diamond (BDD) (Carter and Farrell, 2008; Trautmann et al., 2015; Urtiaga et al., 2015; Gomez-Ruiz et al., 2019; Barisci and Suri, 2020; Garcia-Costa et al., 2020; Pierpaoli et al., 2021) and mixed metal oxides (e.g. Ti_4O_7, PbO_2, Ti/SnO_2–Sb, Ti/SnO_2–Sb–Bi) (Zhuo et al., 2011; Lin et al., 2012; Niu et al., 2012; Wang et al., 2020) have been used for PFOA and PFOS degradation. Among them, BDD is particularly attractive due to its wide potential window, resistance to fouling, excellent corrosion resistance and high overpotential for oxygen generation (Trautmann et al., 2015; Gomez-Ruiz et al., 2019). Previous works involving EAOPs have reported that the first step in PFOA oxidation is the direct electron transfer (DET) at the anode followed by repeated unzipping of CF_2 units through decarboxylation and thermal transformation (Ochiai et al., 2011; Zhuo et al., 2012; Niu et al., 2013; Schaefer et al., 2017; Zhuang et al., 2020). This results in the complete mineralization of PFOA to CO_2 and fluoride ions (F^-).

Till date, very limited research is reported on HFPO-DA (GenX) degradation. Bao et al. (2018) studied the oxidation of GenX based on $SO_4^{•-}$ oxidative degradation using UV/persulfate and reported that <5% of GenX was degraded whereas 26% of PFOA was degraded in 3 h. Adding to that, the <5% GenX degradation was completely attributed to direct UV oxidation and not to sulfate radicals ($SO_4^{•-}$). In their next research (Bao et al., 2020), they studied the oxidation of hexafluoropropylene oxide tetramer acid (HFPO-TeA) using UV/persulfate and reported that HFPO-TeA depolymerized to hexafluoropropylene oxide trimer acid (HFPO-TA) which then depolymerized to HFPO-DA and not further, which supports their previous finding. Pica et al. (2019) studied the electrochemical oxidation of HFPO-DA using BDD anode and reported that $SO_4^{•-}$ was capable of enhancing HFPO-DA oxidation. The effect of $SO_4^{•-}$ in the HFPO-DA degradation is still unclear owing to the contradictory observations reported. The effects of other operating parameters of EAOP (e.g. electrolyte concentration, chloride ions, and current density) that could influence the HFPO-DA degradation have not yet been explored.

In the present study, we investigate the degradation and defluorination efficiency of HFPO-DA using boron-doped diamond anodes in EAOP. This study aims to elucidate the first step in the degradation mechanism of HFPO-DA and to clarify the contradictions previously reported on the role of sulfate radicals. Experiments were performed separately with sodium sulfate and sodium perchlorate to assess the effect of $SO_4^{•-}$. To further provide experimental insight into the degradation pathway, the intermediate products were determined using mass spectrometry in order to propose a possible reaction mechanism. Additionally, the effects of electrolyte concentration, current density, and chloride radicals on the degradation and defluorination efficiency were investigated for the first time to provide in-depth understanding of the degradation. Finally, a comparison is made between the degradation efficiency of HFPO-DA and PFOA using BDD-based EAOP to highlight the effect of steric hindrance in the HFPO-DA molecule.

2. Material and methods

2.1. Chemicals

Hexafluoropropylene oxide dimer acid (HFPO-DA, $C_6HF_{11}O_3$, 97%) was purchased from abcr GmbH, Germany. Perfluorooctanoic acid (PFOA, $C_8HF_{15}O_2$, 95%), sodium sulfate (Na_2SO_4, ≥99%), sodium perchlorate ($NaClO_4$, ≥98%), sodium chloride (NaCl, ≥99%), methanol (CH_3OH, HPLC grade, ≥99.9%), potassium dihydrogen phosphate (KH_2PO_4, EMSURE® ISO) and *tert*-butyl alcohol ($(CH_3)_3COH$, ≥99%) were purchased from Sigma-Aldrich, The Netherlands. N, N-diethyl-p-phenylenediamine (DPD) reagent powder pillows for free chlorine detection were purchased from Hach, The Netherlands. All chemicals were of analytical grade or higher and were used without further purification. All solutions were prepared with ~18 MΩ cm, Type I water (ELGA Purelab UHQ).

2.2. Electrode characterization

Thin-film boron-doped diamond (6 μm thick, boron concentration 2500 ppm) electrodes were purchased from NeoCoat, Switzerland. BDD was coated on a pre-treated niobium substrate (50 mm × 25 mm, 2 mm thick), uniformly on both sides including the edges, using a hot-filament chemical vapor deposition reactor.

Scanning electron microscopy (SEM) measurement was performed with a JEOL JSM-6010LA scanning electron microscope and corresponding images were taken, at a working distance of 10 mm with an accelerating voltage of 10 keV, using a secondary electron detector. Atomic force microscopy (AFM) measurement was done using a Bruker Dimension Edge™ in tapping mode with antimony n-doped silicon tip. The scanned area was 50 μm × 50 μm and the scanning rate was 0.6 Hz. Raman spectroscopy measurement was performed with a Horiba LabRAM HR setup, equipped with an argon ion laser operating at 514 nm and a spectral resolution of ~0.3 cm^{-1}.

2.3. Electrochemical experimentation

Electrochemical oxidation experiments were performed in a single compartment electrochemical cell made of polypropylene. BDD electrode with an effective surface area of 22.6 cm^2 was used as the working anode and a platinum mesh was used as the cathode placed parallel to either side of the anode with an electrode spacing of 10 mm. Experiments were conducted in duplicate in batch mode at room temperature (approximately 22 °C) with an electrolyte volume of 400 mL containing 15 mg L^{-1} of HFPO-DA. To compare between HFPO-DA and PFOA degradation, an equimolar concentration ($[HFPO\text{-}DA]_0 = [PFOA]_0 =$ 45.4 μM) was taken. Electrolytes used in the experiments were sodium sulfate and sodium perchlorate at varying molar concentrations. The concentrations and pH were chosen to simulate the conductivity and pH of groundwater (Bathrellos et al., 2008). The degradation experiments were carried out under constant current conditions. The applied current was supplied by a Keithley 2400 Sourcemeter with a maximum output of 1 A and 200 V and the resulting cell voltage was continuously monitored. The electrolyte solution was stirred using a magnetic stirrer at 300 rpm to increase mass transfer. The initial and final pH (after degradation) of the electrolyte were observed using VWR Dosatest pH test strips. Each experiment was conducted for 4 h with samples collected every 30 min. At the selected intervals, the power source was turned off with the electrolyte being continuously stirred to maintain homogeneity and a sample of 2 mL was collected and stored in a LightSafe polypropylene micro centrifuge tube.

To check for the direct oxidation of chloride and radical scavenger at the BDD anode, linear sweep voltammetry (LSV) measurements were performed using a multichannel Metrohm Autolab potentiostat. They were performed in a three-electrode setup, BDD as the working anode with an active surface area of 1 cm^2, platinum mesh (2 cm × 2 cm) as the cathode, and Ag/AgCl as the reference electrode.

2.4. Analytical methods

To estimate the efficiency of degradation, the concentration of HFPO-DA or PFOA at different time intervals was measured using high performance liquid chromatography (HPLC). The HPLC system (Knauer Smartline) consisted of a degasser, a pump, an automatic sample injector with an injection volume of 10 μL, a column oven (40 °C) and a UV–Vis detector. The HPLC system was equipped with a Phenomenex Kinetex® C18 column (100 mm × 4.6 mm, 2.6 μm). A mixture of 20 mM potassium dihydrogen phosphate (35%) and methanol (65%) was used as mobile phase in isocratic mode. The flow rate was set at 0.6 mL min^{-1} for HFPO-DA and 0.8 mL min^{-1} for PFOA. The detection was monitored at λ = 200 nm. The UV excitation wavelength of HFPO-DA and PFOA was checked with a Shimadzu UV-2600 (Fig. S1).

To confirm the complete degradation/mineralization of HFPO-DA and PFOA, the concentration of fluoride (F^-) was measured using an ion-chromatograph system (DX-120, DIONEX) consisting of a separation column (IonPak AS12A, 200 mm × 4 mm) and a suppressed conductivity detector. The mobile phase consisted of an aqueous solution of 1 mM Na_2CO_3 and 1 mM $NaHCO_3$ and the flow rate was set at 1.3 mL min^{-1}. Other anions such as chloride and sulfate were also measured. The retention times of F^-, Cl^- and SO_4^{2-} were 2.9, 3.5 and 13 min, respectively.

The intermediates of HFPO-DA degradation were qualitatively analyzed using an ultra-performance liquid chromatography coupled with high-resolution mass spectrometry (LC-MS). Samples from individual time points were diluted 1:100 with H_2O and 2.5 μL of each sample was analyzed. Reverse phase chromatography was performed using a UPLC BEH (1.0 mm × 100 mm, 1.7 μm, Waters, Acquity) separation column coupled online to a QE plus Orbitrap mass spectrometer (Thermo Scientific, Germany) operated in polarity switching, thereby alternating ES+ and ES- modes. Buffer A consisted of 0.1% formic acid in LC-MS grade water and buffer B consisted of 0.1% formic acid in LC-MS grade acetonitrile. A flow rate of 50 μL min^{-1} was maintained using an Acquity Ultra Performance LC pump system (Waters, Milford, United States). After sample injection, 10% B was kept constant over 2.5 min, followed by a linear gradient to a solvent composition of 90% B over 10 min, which was kept constant for further 2.5 min until back-equilibration to solvent start conditions. The full scan was acquired over the mass range of 75–500 m/z at a resolution of 70k and an AGC target of 1e6. External calibration was performed using the Pierce LTQ Velos ESI Positive Ion Calibration Solution before performing the sample analysis. Sample runs were analyzed using QualBrowser part of the Thermo Scientific Xcalibur software tool.

3. Results and discussion

3.1. Characterization of the BDD electrode

The SEM image in Fig. 1a illustrates the surface morphology of the thin-film BDD electrode. The irregular topography observed is due to the roughness generated during pretreatment of the niobium surface prior to deposition. The BDD surface represents a cauliflower-like morphology (Castro et al., 2012) likely caused by renucleation (Buijnsters and Vázquez, 2011) occurring during the growth of the polycrystalline diamond coating. The average surface grain size of the BDD coating was between 0.5 and 1 μm. Irrespective of the Nb roughness, the diamond grains were uniformly distributed and no coating defects (e.g. pinholes or delamination) were observed. Using AFM, the topography of the BDD coating with a root-mean square surface roughness of about 860 nm and a maximum peak height of 5.44 μm was observed (Fig. S2). The ratio of surface area to projected area was calculated to be 1.11. Fig. 1b shows the Raman spectrum obtained from the BDD surface. At least, five different signals can be distinguished. The origin of the two broad bands located at ca. 491 and 1239 cm^{-1} remains poorly understood (Mortet et al., 2019) but they are frequently attributed to boron inclusion in the diamond lattice (B–C vibrational modes) and the Fano resonance from lattice impurities due to boron doping (Sartori et al., 2018), respectively. The sharp peak at 1330 cm^{-1} corresponds to diamond one-phonon line (Sartori et al., 2018). The shoulder peak observed around 1355 cm^{-1} and the peak at 1587 cm^{-1} are the so-called D- and G-bands (Merlen et al., 2017), which originate from sp^2 carbon present in both disordered/defective and crystalline forms of graphite trapped in the grain boundaries. Since sp^2 carbon mainly resides in the grain boundaries, small average diamond grain size leads to a relatively low sp^3/sp^2 ratio which plays an important role in determining the electrode performance (Macpherson, 2015; Liu et al., 2021) in EAOP.

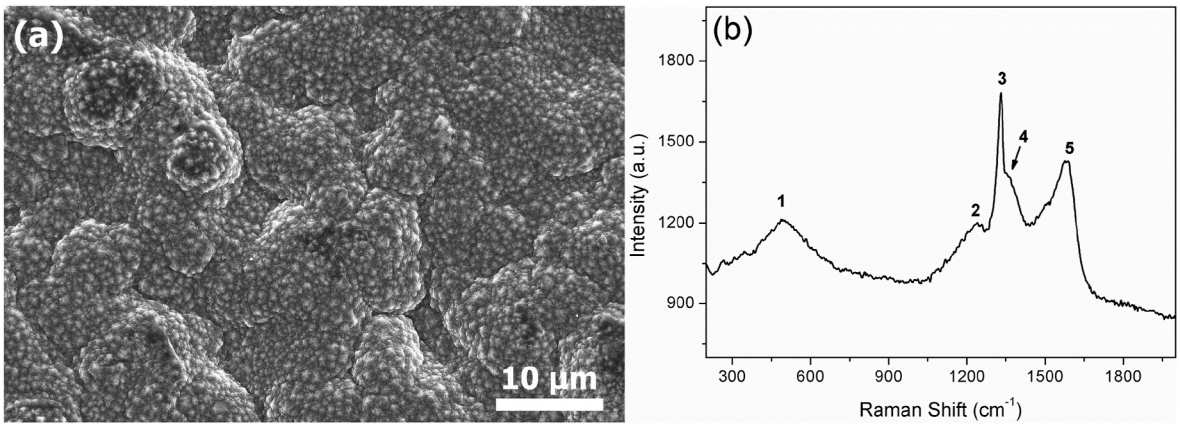

Fig. 1. Characterization of the pristine BDD anode surface (a) SEM micrograph (b) visible micro-Raman spectrum. The Raman signals labeled 1–5 correspond to signals from B–C vibrational modes (1), Fano resonance (2), diamond (3), and the D-band (4) and G-band (5) of graphite, respectively.

3.2. Electrochemical degradation of HFPO-DA

3.2.1. Role of sulfate radicals

Sulfate radicals formed due to DET at the anode (Ahmadi et al., 2021) are highly reactive owing to their high redox potential (2.5–3.1 V vs SHE). The average lifetime of $SO_4^{\bullet-}$ is 30–40 μs which is much longer than $OH^{\bullet}$ (20 ns) (Ghanbari and Moradi, 2017). To probe the role of sulfate radicals, HFPO-DA degradation was performed separately in Na_2SO_4 and $NaClO_4$ electrolyte since $NaClO_4$ is considered inert during anodic oxidation. The degradation was conducted in $NaClO_4$ electrolyte with the same ionic conductivity (2.34 mS cm^{-1} @ 22 °C) as 0.01 M Na_2SO_4. The anodic potentials were higher than the oxidation potential of sulfate ion to ensure generation of $SO_4^{\bullet-}$ (Fig. S3). Fig. 2a shows the effect of electrolyte type on the degradation of HFPO-DA. It was observed that the degradation rate was almost similar in both electrolytes reaching a degradation of 91% (Na_2SO_4) and 93% ($NaClO_4$) after 4 h. The reaction followed pseudo-first order kinetics (Fig. 2a inset) and the apparent rate constants (k_{app}) in Na_2SO_4 and $NaClO_4$ electrolytes were 0.0106 and 0.0113 min^{-1}. Experiments were also conducted at a higher ionic conductivity (9.77 mS cm^{-1} @ 22 °C) in both electrolytes and a similar trend was observed (Fig. S4). Again, the degradation rate was virtually identical for both electrolytes but the overall degradation (82% after 4 h) was lower than at lower ionic conductivity. This can be ascribed to the decrease in voltage with increase in ionic conductivity which directly reduces the electron transfer rate. From the data in Fig. 2a and S4, we can conclude that sulfate radicals are ineffective in HFPO-DA degradation which supports previous findings using UV/persulfate (Bao et al., 2018, 2020). This is in contrast with previous findings using EAOP (Pica et al., 2019) in which sodium chloride and methanol were used to study the effect of sulfate radicals. It has to be noted that the direct oxidation of chloride and methanol (a radical scavenger) at the anode can occur as competing reactions to the direct oxidation of HFPO-DA and hence hinder its degradation.

Fig. 2b shows the effect of electrolyte on the percentage of fluoride recovered during the degradation of HFPO-DA. After 4 h, a defluorination of 80% and 84% was achieved in Na_2SO_4 and $NaClO_4$ electrolytes, respectively. Since the generated sulfate radicals can hinder the oxidation of intermediate products through competing reactions (Pica et al., 2019), the defluorination efficiency was comparatively higher in $NaClO_4$ electrolyte.

3.2.2. Effect of electrolyte concentration

Experiments in different electrolyte concentrations ranging from 0.005 to 0.05 M Na_2SO_4 were conducted as shown in Fig. 3. After 4 h, the degradation of HFPO-DA reached 96%, 92%, and 81% in corresponding electrolyte concentrations of 0.005, 0.01, and 0.05 M (Fig. 3a). Fig. 3b shows the pseudo-first order kinetics followed. The corresponding

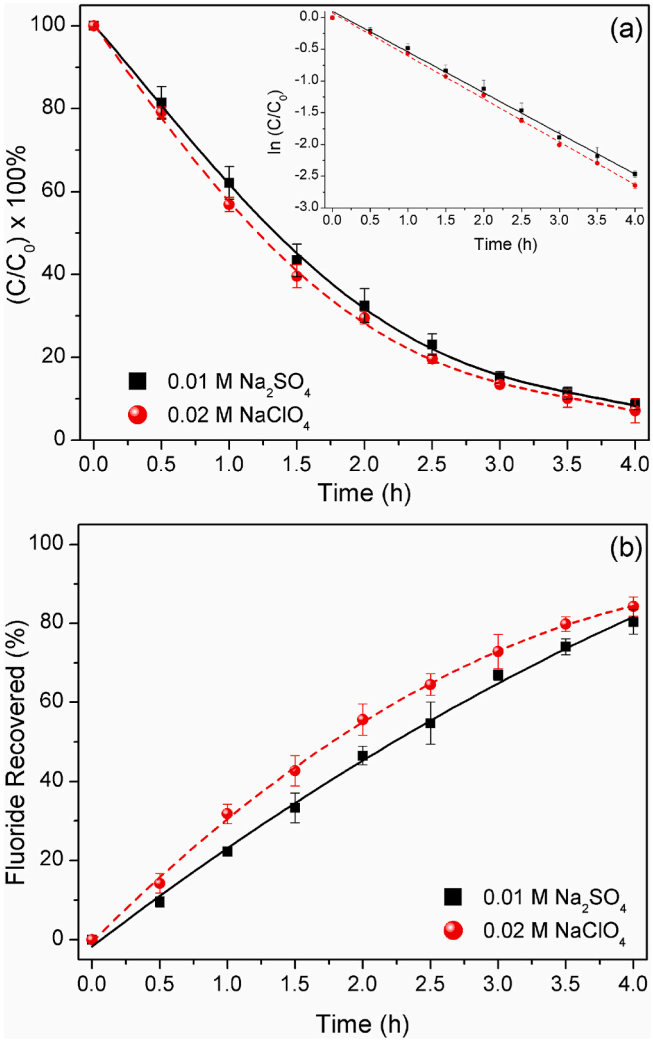

Fig. 2. Effect of electrolyte on (A) HFPO-DA degradation (inset showing the pseudo-first order kinetic analysis) and (B) defluorination. Current density = 20 mA cm^{-2}, pH = 7, $[HFPO\text{-}DA]_0$ = 15 mg L^{-1}, electrolyte: 0.01 M Na_2SO_4 and 0.02 M $NaClO_4$, ionic conductivity = 2.34 mS cm^{-1} @ 22 °C.

kinetic constant (k_{app}) reduced from 0.0129 to 0.0068 min^{-1} with increasing electrolyte concentration from 0.005 to 0.05 M. After degradation, it was worth noting that the final pH increased from 7 to 10

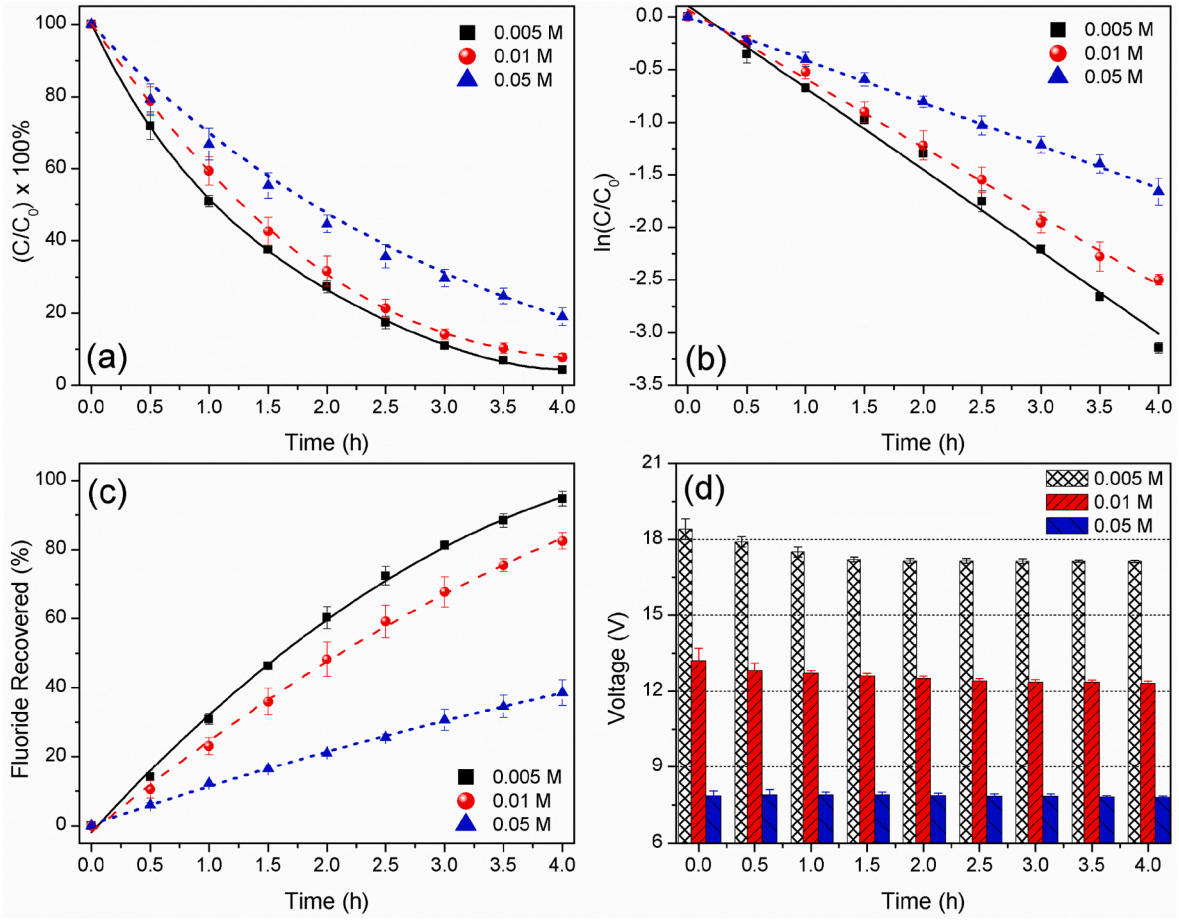

Fig. 3. Effect of electrolyte concentration on (A) HFPO-DA degradation with (B) corresponding pseudo-first order kinetic analysis, (C) defluorination, and (D) cell voltage. Current density = 20 mA cm^{-2}, pH = 7, $[HFPO\text{-}DA]_0$ = 15 mg L^{-1}, electrolyte: Na_2SO_4.

with increase in electrolyte concentration which could hinder the degradation. This is due to the competitive reactions between DET of SO_4^{2-} and OH^- at the anode to maintain the balance of electron flow (Eqs. (1)–(3)) and the hydrogen evolution reaction at the cathode that leads to formation of OH^- (Eq. (4)).

$$SO_4^{2-} \rightarrow SO_4^{\bullet-} + e^- \quad (1)$$

$$SO_4^{\bullet-} + SO_4^{\bullet-} \rightarrow S_2O_8^{2-} \quad (2)$$

$$OH^- \rightarrow OH^{\bullet} + e^- \quad (3)$$

$$2H_2O + 2e^- \rightarrow 2OH^- + H_2 \quad (4)$$

Fig. 3c shows the effect of electrolyte concentration on the percentage of fluoride recovered during the degradation. After 4 h, a defluorination of 95%, 82%, and 39% was achieved in 0.005, 0.01, and 0.05 M Na_2SO_4 electrolytes, respectively. This supports the above-described fact that the degradation of intermediates is hindered to a great extent through competing reactions occurring due to the electrosorption of sulfate ions at the anode to generate sulfate radicals (Eq. (1)). In addition, with increase in electrolyte concentration, the resulting cell voltage reduces which directly reduces the effective electron transfer. The resulting cell voltage at different electrolyte concentrations is shown in Fig. 3d. In 0.005 and 0.01 M experiments, the voltage decreased by 0.9 and 0.5 V after 1 h of degradation due to the additional conductivity of recovered fluoride ions. When the electrolyte concentration was increased from 0.05 to 0.1 M Na_2SO_4, the resulting cell voltage reduced from 7.8 to 7.4 V (not shown) which was very small compared to the other voltage differences between electrolyte concentrations in Fig. 3d. The degradation in 0.1 M Na_2SO_4 followed zero order kinetics due to the high electrolyte conductivity which nearly eliminates electromigration based mass transfer of HFPO-DA (Fig. S5). HFPO-DA (pKa = 2.84) (Mullin et al., 2019) dissociates into $C_6F_{11}O_3^-$ and H^+ in water and at high background electrolyte conductivity, the reaction is diffusion-controlled following zero order kinetics.

3.2.3. Effect of current density

To study the effect of current density on HFPO-DA degradation, different current densities ranging from 5 to 30 mA cm^{-2} were applied. Fig. 4a shows the effect of current density on HFPO-DA degradation. After 4 h, the degradation reached 77%, 85%, 91%, and 97% with corresponding current densities of 5, 10, 20, and 30 mA cm^{-2}. The corresponding kinetic constant follows the order of 0.0059 < 0.0077 < 0.0105 < 0.0150 min^{-1} with increasing current density from 5 to 30 mA cm^{-2}. Fig. 4b shows the effect of current density on the percentage of fluoride recovered during the degradation. After 4 h, a defluorination of 63%, 72%, 86%, and 95% was achieved at current densities of 5, 10, 20, and 30 mA cm^{-2}, respectively. Increasing applied current density leads to increasing electron transfer rate and generation of reactive oxidants (e.g. $OH^{\bullet}$), thus faster HFPO-DA degradation and defluorination is achieved.

3.2.4. Effect of chloride and reactive chlorine species

To study the effect of chloride and reactive chlorine species on HFPO-DA degradation, experiments were conducted in different concentrations of NaCl ranging from 0 to 15 mM. To minimize the effect of voltage reduction due to addition of NaCl, 0.02 M Na_2SO_4 was added as a background electrolyte. Linear sweep voltammetry (LSV) profiles confirm the direct oxidation of Cl^- at the BDD anode (Fig. S6). The direct

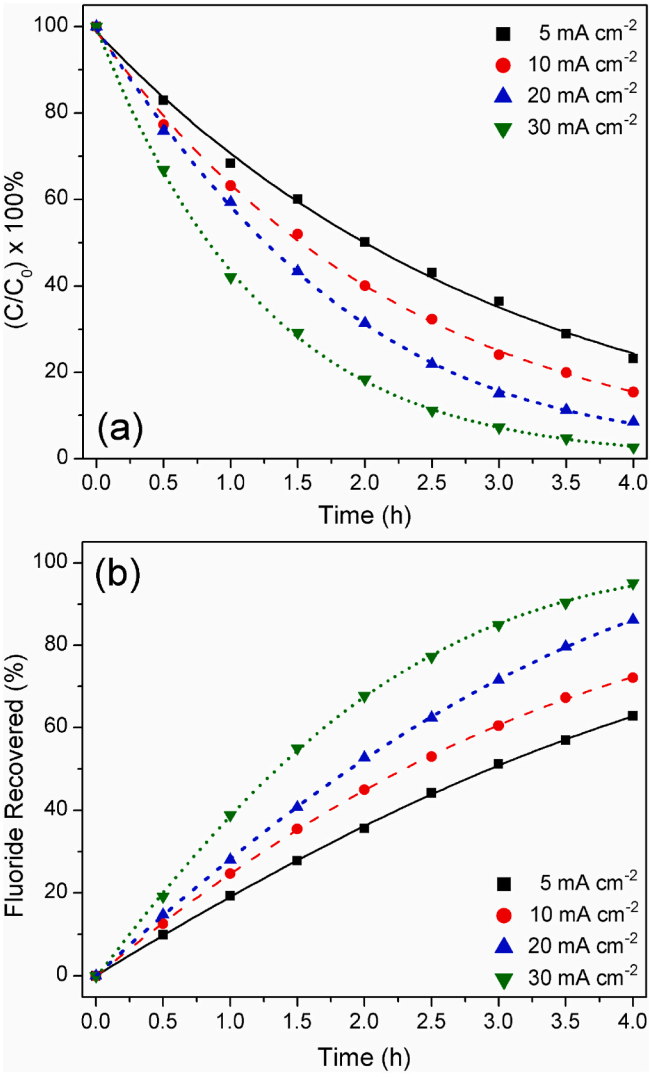

Fig. 4. Effect of applied current density on (a) HFPO-DA degradation and (b) defluorination. pH = 7, $[HFPO\text{-}DA]_0$ = 15 mg L^{-1}, electrolyte: 0.01 M Na_2SO_4, ionic conductivity = 2.34 mS cm^{-1} @ 22 °C.

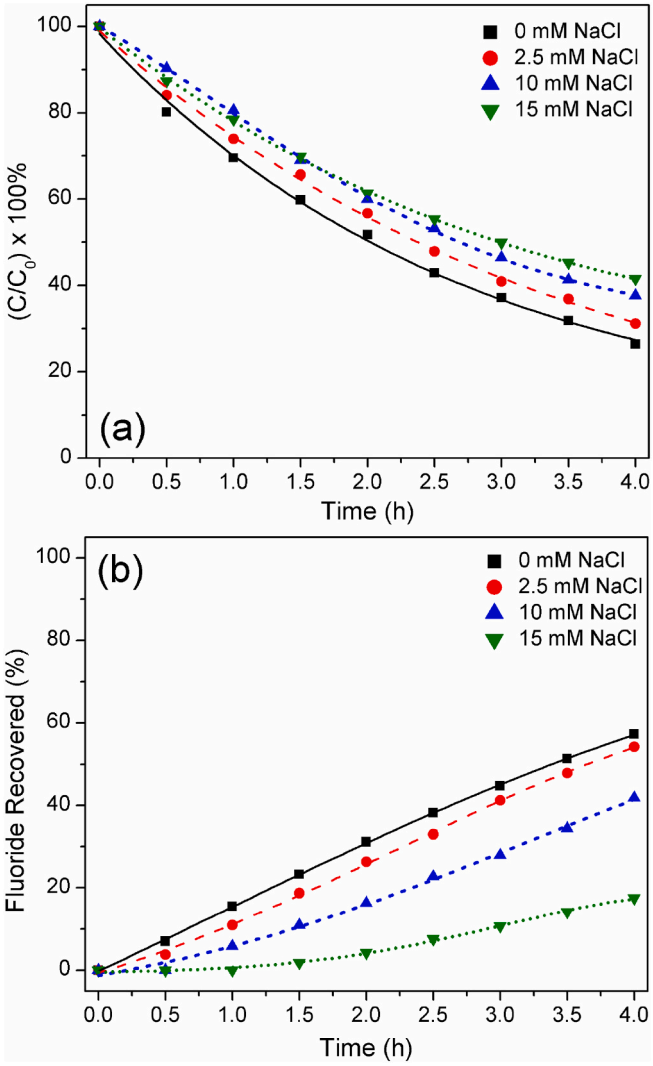

Fig. 5. Effect of chloride on (a) HFPO-DA degradation (b) defluorination. Current density = 10 mA cm^{-2}, pH = 7, $[HFPO\text{-}DA]_0$ = 15 mg L^{-1}, background electrolyte: 0.02 M Na_2SO_4.

oxidation of Cl^- is further confirmed with the decrease in Cl^- concentration during degradation (Fig. S7). Fig. 5a shows the effect of chloride on HFPO-DA degradation. After 4 h, the degradation reached 74%, 69%, 62%, and 58% in corresponding NaCl concentrations of 0, 2.5, 10, and 15 mM. This shows that Cl^- inhibited HFPO-DA degradation to a considerable extent by occupying active sites on the electrode. Formation of free chlorine was confirmed by use of DPD reagent (Schwenke et al., 2019) which is oxidized by free chlorine to give a pink color (Fig. S8).

Fig. 5b shows the effect of chloride on the percentage of fluoride recovered during the degradation. After 4 h, a defluorination of 57%, 54%, 42%, and 17% was achieved in 0, 2.5, 10, and 15 mM NaCl electrolytes, respectively. Since oxidation of chloride (E° = 2.0 V, from Fig. S6) occurs at a lower potential than $OH^\bullet$ generation (E° = 2.8 V), $OH^\bullet$ formation is hindered due to competing reactions at the anode and also due to consumption of $OH^\bullet$ by chloride species to form by-products (Barazesh et al., 2016). However, previous work demonstrated that DET of Cl^- and its reaction with $OH^\bullet$ can lead to the formation of reactive chlorine species ($Cl^\bullet$, Cl_2, ClO^-) (Eqs. (5)–(7)) that accelerated the degradation of PFOS (Wang et al., 2020). Electrooxidation of Cl^- using BDD anode can also lead to the formation of unwanted by-products by the formation of chlorate and perchlorate (Eq. (8)).

$$Cl^- \rightarrow (Cl_{ads}^\bullet) + e^- \quad (5)$$

$$Cl^\bullet + Cl^\bullet \rightarrow Cl_2 \quad (6)$$

$$Cl^\bullet + OH^\bullet \rightarrow ClO^- + H^+ \quad (7)$$

$$Cl^- \rightarrow ClO^- \rightarrow ClO_2^- \rightarrow ClO_3^- \rightarrow ClO_4^- \quad (8)$$

3.2.5. *Effect of radical scavengers*

To show that $OH^\bullet$ plays an important role in the cleaving of C–F bonds, radical scavengers were used in a further experiment. *Tert*-butyl alcohol (TBA) lacking α-hydrogen is commonly used as $OH^\bullet$ scavenger due to its higher reactivity with $OH^\bullet$ with a reaction rate constant of 3.8–7.6 × 10^8 M^{-1} s^{-1} (Buxton et al., 1988; Barazesh et al., 2016; Schaefer et al., 2017). A molar concentration of 0.1 M TBA was added to 0.01 M Na_2SO_4 electrolyte containing 15 mg L^{-1} HFPO-DA. After 2 h of degradation, it was observed that no fluoride was recovered and after 4 h, only 5% of fluoride was recovered. Thus, 0.1 M TBA was sufficient enough to scavenge most of the generated $OH^\bullet$. This demonstrates that the reaction of $OH^\bullet$ with HFPO-DA to form an unstable alcohol is necessary for complete mineralization of HFPO-DA. Fig. S9 shows the effect of TBA addition on the HFPO-DA degradation. It has to be noted that $OH^\bullet$ reacts rapidly with compounds through hydrogen abstraction

and addition to unsaturated bonds and not through electron transfer mechanism (Farhat et al., 2015). Since the first step in HFPO-DA degradation is the direct electron transfer (DET), the decrease in degradation efficiency is due to the direct oxidation of TBA competing with DET of HFPO-DA by occupying the active sites on the BDD anode. LSV profiles further confirm the oxidation of TBA at the BDD anode (Fig. S10).

3.2.6. Comparison between PFOA and HFPO-DA degradation

Fig. 6 shows the comparison between PFOA and HFPO-DA on degradation and defluorination. After 1 h, 57% of PFOA was degraded whereas only 38% of HFPO-DA was degraded. This indicates that the presence of $–CF_3$ branch at the α-position hinders effective electron transfer from the carboxylic head group. Also, sulfate radicals were observed ineffective due to the same reason, thus introducing complexity in the first step of HFPO-DA degradation. It can be observed that in the first hour, more fluoride was generated from PFOA than from HFPO-DA degradation which is due to the higher efficiency of PFOA degradation. After 2 h, however, the fluoride generated from PFOA degradation was lower than from HFPO-DA. The percentage of fluoride recovered from HFPO-DA after 4 h was 20% higher than from PFOA. These observations bring us to a conclusion that the direct electron transfer from HFPO-DA to the anode is the rate-determining step in HFPO-DA degradation and that HFPO-DA shows a faster defluorination than PFOA under identical conditions.

3.3. Degradation mechanism of HFPO-DA

The mechanism of electrochemical degradation of HFPO-DA using BDD anodes was derived using LC-MS analysis. A full scan MS spectrum of a sample collected after 2.5 h of degradation is shown in Fig. S11. The spectrum of an intermediate product, namely pentafluoropropionic acid (PFA, $CF_3CF_2COO^-$) and its corresponding HPLC chromatograph is shown in Fig. S12. Density functional theory (DFT) calculations indicated that the carboxylic group is the preferred site for direct electron transfer and the oxidative degradation does not lead to the splitting of ether bond in HFPO-DA (Pica et al., 2019). Bao et al. (2020) proposed that the oxidative degradation of HFPO-TeA (TeA-tetramer acid) and HFPO-TA (TA-trimer acid) led to the split of ether bond at the non-ionic end whereas the same was not observed in HFPO-DA with only one ether bond.

From the above, we derive the possible oxidative degradation pathway of HFPO-DA as illustrated in Fig. 7. The first step in HFPO-DA degradation is the direct electron transfer (DET) at the anode surface **(1)** leading to the formation of an alkyl radical via Kolbe decarboxylation **(2)**. The formed radical reacts with $OH^•$ **(3)** to form a thermally unstable alcohol which due to hydrogen abstraction **(4)** undergoes $–CF_3$ elimination to form acyl fluoride ($C_4F_8O_2$). $C_4F_8O_2$ undergoes hydrolysis **(5)** to form an acid ($C_4F_7O_3^-$) through another F^- elimination. This intermediate again undergoes reaction (1) to (3) to form an unstable alcohol **(6)** which through HF elimination **(7)** leads to the formation of a shorter acyl fluoride (C_3F_6O). This acyl fluoride undergoes hydrolysis **(8)** to form the second intermediate pentafluoropropionic acid (PFA, $CF_3CF_2COO^-$). The formation of subsequent alkyl radical, alcohol, acyl fluoride and acid is labeled as 4A process (Bao et al., 2020). The intermediate PFA through 4A process **(9)** leads to the formation of the third intermediate trifluoroacetic acid (TFA, CF_3COO^-) through $–CF_2$ unzipping. In the final step, TFA through unzipping **(10)** leads to the formation of F^- and CO_2. Accordingly, HFPO-DA completely mineralizes to F^- and CO_2 through the formation of three intermediates, namely $C_4F_7O_3^-$, PFA and TFA. The formation of PFA and TFA was not reported previously in the HFPO-DA degradation pathway proposed by Pica et al. (2019) using DFT calculations. Hence, the experimental determination of these intermediates gives more insight into the closest feasible HFPO-DA degradation pathway.

In the case of PFOA, which is a linear PFAS isomer, the number of intermediates formed are six as illustrated in Fig. S13. Hence, the number of intermediates in HFPO-DA is comparatively less which leads to faster defluorination rate, as was observed experimentally (Fig. 6).

The findings of our study demonstrate the complexity in HFPO-DA degradation due to the presence of $–CF_3$ branch and its resistance to sulfate and chloride radicals. However, electrochemical degradation of HFPO-DA using BDD anode has resulted in the complete mineralization to CO_2 and F^-. This supports EAOP using BDD anode as a promising approach towards sustainable and effective water treatment. EAOPs can be easily implemented in the existing fluoropolymer production plants that release various PFAS varieties into the water stream (Gebbink and van Leeuwen, 2020). Hence, EAOPs help to drastically reduce their discharge into the environment through the complete mineralization of PFAS.

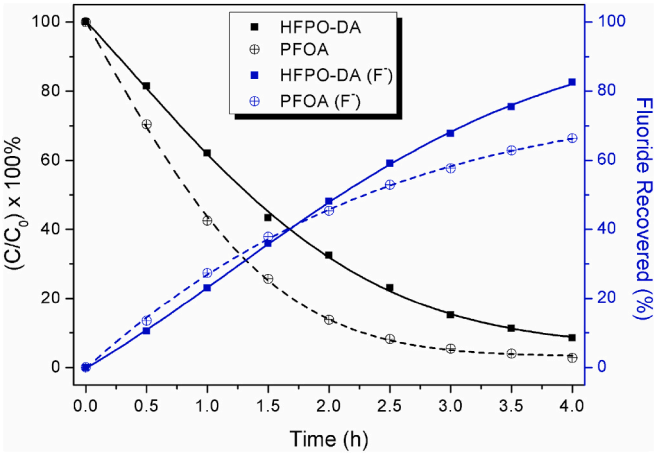

Fig. 6. Comparison between HFPO-DA and PFOA on degradation and defluorination. Current density = 20 mA cm^{-2}, pH = 7, $[HFPO\text{-}DA]_0$ = $[PFOA]_0$ = 45.4 μM, electrolyte: 0.01 M Na_2SO_4.

4. Conclusions

This study examined the electrochemical degradation of HFPO-DA using BDD anodes with an experimental insight into degradation influencing parameters. The primary conclusions drawn from this study can be summarized as follows.

- HFPO-DA completely mineralizes to CO_2 and F^- via formation of three intermediates.
- Direct electron transfer was observed to be the rate-determining step in HFPO-DA degradation.
- Sulfate radicals are ineffective in HFPO-DA degradation due to the steric hindrance by the $–CF_3$ branch which blocks the trajectory of $SO_4^{•-}$.
- Increase of sulfate concentration decreased the degradation and defluorination efficiency due to decrease in cell voltage and deceleration in oxidation of intermediate products in presence of $SO_4^{•-}$, respectively.
- Increase of current density increased the degradation and defluorination efficiency due to effective electron transfer and increased $OH^•$ production.
- Increase of chloride concentration decreased the degradation and defluorination efficiency due to competing reactions at anode and quenching of $OH^•$ by Cl^-.
- By use of radical scavengers, it was observed that $OH^•$ is crucial for complete mineralization.
- By comparing degradation of HFPO-DA with that of PFOA, it was observed that the presence of the $–CF_3$ branch increased the complexity of electron transfer in HFPO-DA degradation even

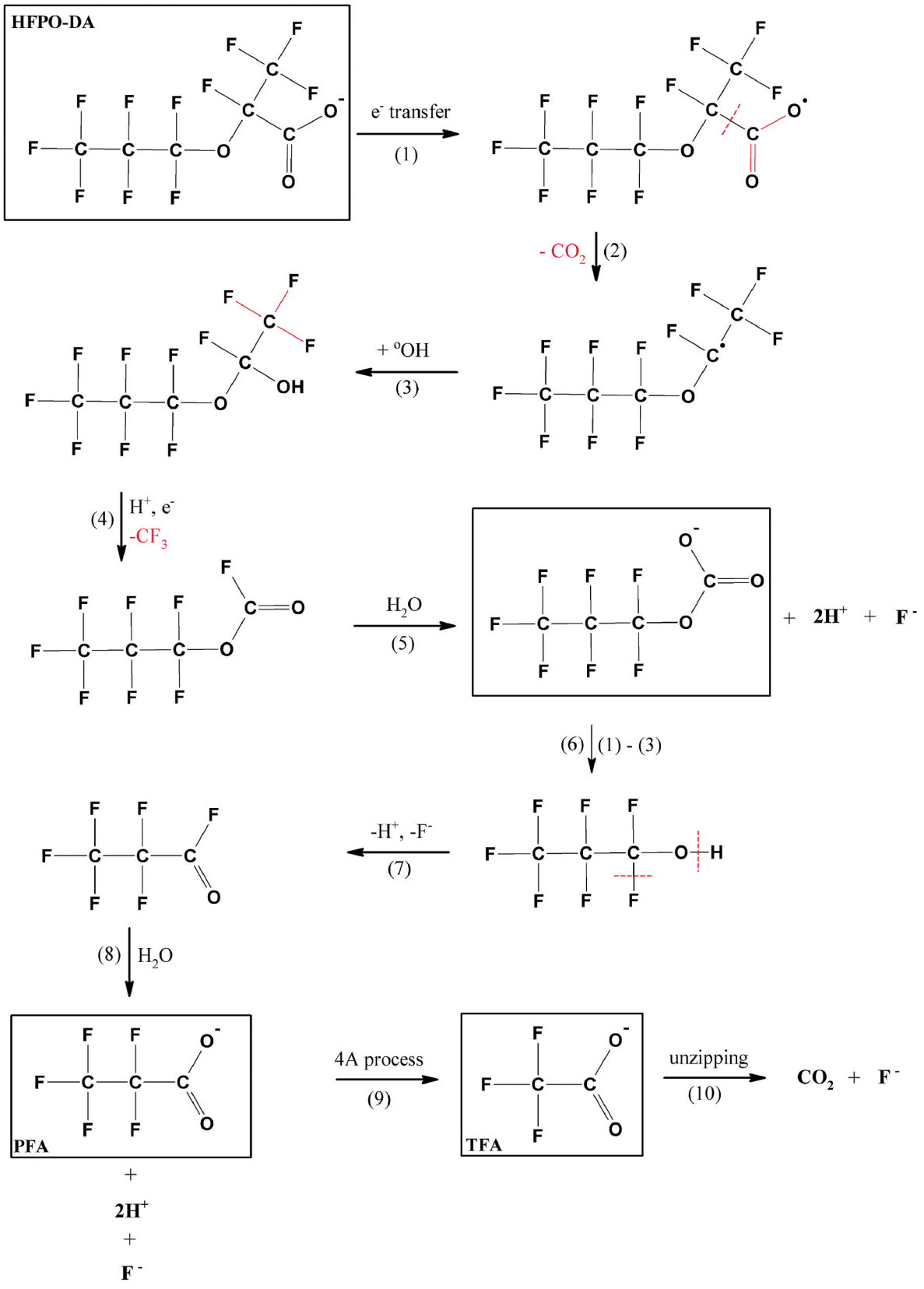

Fig. 7. Proposed oxidative degradation pathway of HFPO-DA through determination of intermediates using LC-MS analysis. For complete mineralization, HFPO-DA degrades through successive formation of three intermediates to form CO_2 and F^-. PFA – Pentafluoropropionic acid and TFA – Trifluoroacetic acid.

though the defluorination rate was faster for HFPO-DA than for PFOA due to lesser number of intermediates.

Declaration of competing interest

The authors declare that they have no known competing financial interests or personal relationships that could have appeared to influence the work reported in this paper.

Acknowledgements

The authors would like to thank Dr. Martin Pabst and Mr. Michel van den Brink from the Departments of Biotechnology and Process & Energy of Delft University of Technology for the mass spectrometry analysis and the assistance in the HPLC and IC analyses, respectively. D.S.B and J.G.B acknowledge Mr. Zhichao Liu for the assistance in setting up the initial degradation experiments. J.G.B acknowledges the Dutch Research Council (NWO) for funding through the Open Technology Programme (project no. 16361).

Appendix A. Supplementary data

Supplementary data to this article can be found online at https://doi.org/10.1016/j.chemosphere.2021.132417.

Credit author contribution statement

Diwakar Suresh Babu: Conceptualization, Investigation, Formal analysis, Visualization, Writing – original draft. Johannes M.C. Mol: Supervision, Resources, Writing – review & editing. Josephus G. Buijnsters: Conceptualization, Supervision, Resources, Writing – review & editing, Funding acquisition, Project administration.

References

Ahmadi, M.F., da Silva, Á.R.L., Martínez-Huitle, C.A., Bensalah, N., 2021. Understanding the electro-catalytic effect of benzene ring substitution on the electrochemical oxidation of aniline and its derivatives using BDD anode: cyclic voltammetry, bulk electrolysis and theoretical calculations. Electrochim. Acta 369, 137688. https://doi.org/10.1016/j.electacta.2020.137688.

Amor, C., Marchão, L., Lucas, M.S., Peres, J.A., 2019. Application of advanced oxidation processes for the treatment of recalcitrant agro-industrial wastewater: a review. Water 11, 205. https://doi.org/10.3390/w11020205.

Appleman, T.D., Dickenson, E.R.V., Bellona, C., Higgins, C.P., 2013. Nanofiltration and granular activated carbon treatment of perfluoroalkyl acids. J. Hazard Mater. 260, 740–746. https://doi.org/10.1016/j.jhazmat.2013.06.033.

Baabish, A., Sobhanei, S., Fiedler, H., 2021. Priority perfluoroalkyl substances in surface waters - a snapshot survey from 22 developing countries. Chemosphere 273, 129612. https://doi.org/10.1016/j.chemosphere.2021.129612.

Banks, D., Jun, B.-M., Heo, J., Her, N., Park, C.M., Yoon, Y., 2020. Selected advanced water treatment technologies for perfluoroalkyl and polyfluoroalkyl substances: a review. Separ. Purif. Technol. 231, 115929. https://doi.org/10.1016/j.seppur.2019.115929.

Bao, Y., Cagnetta, G., Huang, J., Yu, G., 2020. Degradation of hexafluoropropylene oxide oligomer acids as PFOA alternatives in simulated nanofiltration concentrate: effect of molecular structure. Chem. Eng. J. 382, 122866. https://doi.org/10.1016/j.cej.2019.122866.

Bao, Y., Deng, S., Jiang, X., Qu, Y., He, Y., Liu, L., Chai, Q., Mumtaz, M., Huang, J., Cagnetta, G., Yu, G., 2018. Degradation of PFOA substitute: GenX (HFPO–DA ammonium salt): oxidation with UV/persulfate or reduction with UV/sulfite? Environ. Sci. Technol. acs.est.8b02172. https://doi.org/10.1021/acs.est.8b02172.

Baran, J.R., Erik Kissa (Consultant, Wilmington, DE), 2001. Fluorinated surfactants and repellents, 2001. xiv + 616 pp. $195.00. In: Revised and Expanded Surfactant Science Series, second ed., vol. 97. Marcel Dekker, New York, ISBN 0-8247-0472-X. https://doi.org/10.1021/ja015260a. J. Am. Chem. Soc. 123, 8882–8882.

Barazesh, J.M., Prasse, C., Sedlak, D.L., 2016. Electrochemical transformation of trace organic contaminants in the presence of halide and carbonate ions. Environ. Sci. Technol. 50, 10143–10152. https://doi.org/10.1021/acs.est.6b02232.

Barisci, S., Suri, R., 2020. Electrooxidation of short and long chain perfluorocarboxylic acids using boron doped diamond electrodes. Chemosphere 243, 125349. https://doi.org/10.1016/j.chemosphere.2019.125349.

Bathrellos, G.D., Skilodimou, H.D., Kelepertsis, A., Alexakis, D., Chrisanthaki, I., Archonti, D., 2008. Environmental research of groundwater in the urban and suburban areas of Attica region, Greece. Environ. Geol. 56, 11–18. https://doi.org/10.1007/s00254-007-1135-6.

Beekman, M., Zweers, P., Muller, A., de Vries, W., Janssen, P., Zeilmaker, M., 2016. Evaluation of Substances Used in the GenX Technology by Chemours. Dordrecht. RIVM Lett. Repp. 2016–0174.

Boo, C., Wang, Y., Zucker, I., Choo, Y., Osuji, C.O., Elimelech, M., 2018. High performance nanofiltration membrane for effective removal of perfluoroalkyl substances at high water recovery. Environ. Sci. Technol. 52, 7279–7288. https://doi.org/10.1021/acs.est.8b01040.

Brandsma, S.H., Koekkoek, J.C., van Velzen, M.J.M., de Boer, J., 2019. The PFOA substitute GenX detected in the environment near a fluoropolymer manufacturing plant in The Netherlands. Chemosphere 220, 493–500. https://doi.org/10.1016/j.chemosphere.2018.12.135.

Buijnsters, J.G., Vázquez, L., 2011. Growth dynamics of nanocrystalline diamond thin films deposited by hot filament chemical vapor deposition: influence of low sticking and renucleation processes. J. Phys. Chem. C 115, 9681–9691. https://doi.org/10.1021/jp201919r.

Buxton, G.V., Greenstock, C.L., Helman, W.P., Ross, A.B., 1988. Critical review of rate constants for reactions of hydrated electrons, hydrogen atoms and hydroxyl radicals (·OH/·O − in aqueous solution. J. Phys. Chem. Ref. Data 17, 513–886. https://doi.org/10.1063/1.555805.

Carter, K.E., Farrell, J., 2008. Oxidative destruction of perfluorooctane sulfonate using boron-doped diamond film electrodes. Environ. Sci. Technol. 42, 6111–6115. https://doi.org/10.1021/es703273s.

Castro, M., Cuerno, R., Nicoli, M., Vázquez, L., Buijnsters, J.G., 2012. Universality of cauliflower-like fronts: from nanoscale thin films to macroscopic plants. New J. Phys. 14, 103039. https://doi.org/10.1088/1367-2630/14/10/103039.

Chemours named in GenX lawsuit, 2017. C&EN Glob. Enterp. 95, 11. https://doi.org/10.1021/cen-09541-notw11, 11.

Cheryl Hogue, 2019. Guide to PFAS in our environment debuts. C&EN Glob. Enterp. 97, 12. https://doi.org/10.1021/cen-09721-polcon2, 12.

Conder, J.M., Hoke, R.A., Wolf, W. de, Russell, M.H., Buck, R.C., 2008. Are PFCAs bioaccumulative? A critical review and comparison with regulatory criteria and persistent lipophilic compounds. Environ. Sci. Technol. 42, 995–1003. https://doi.org/10.1021/es070895g.

Cousins, I.T., Vestergren, R., Wang, Z., Scheringer, M., McLachlan, M.S., 2016. The precautionary principle and chemicals management: the example of perfluoroalkyl acids in groundwater. Environ. Int. 94, 331–340. https://doi.org/10.1016/j.envint.2016.04.044.

Daly, E.R., Chan, B.P., Talbot, E.A., Nassif, J., Bean, C., Cavallo, S.J., Metcalf, E., Simone, K., Woolf, A.D., 2018. Per- and polyfluoroalkyl substance (PFAS) exposure assessment in a community exposed to contaminated drinking water, New Hampshire, 2015. Int. J. Hyg Environ. Health 221, 569–577. https://doi.org/10.1016/j.ijheh.2018.02.007.

Davis, K.L., Aucoin, M.D., Larsen, B.S., Kaiser, M.A., Hartten, A.S., 2007. Transport of ammonium perfluorooctanoate in environmental media near a fluoropolymer manufacturing facility. Chemosphere 67, 2011–2019. https://doi.org/10.1016/j.chemosphere.2006.11.049.

Domingo, J.L., Nadal, M., 2019. Human exposure to per- and polyfluoroalkyl substances (PFAS) through drinking water: a review of the recent scientific literature. Environ. Res. 177, 108648. https://doi.org/10.1016/j.envres.2019.108648.

ECHA, 2020. Candidate List of Substances of Very High Concern for Authorisation [WWW Document] (accessed 1.22.21). https://echa.europa.eu/candidate-list-table.

Farhat, A., Keller, J., Tait, S., Radjenovic, J., 2015. Removal of persistent organic contaminants by electrochemically activated sulfate. Environ. Sci. Technol. https://doi.org/10.1021/acs.est.5b02705.

Flores, C., Ventura, F., Martin-Alonso, J., Caixach, J., 2013. Occurrence of perfluorooctane sulfonate (PFOS) and perfluorooctanoate (PFOA) in N.E. Spanish surface waters and their removal in a drinking water treatment plant that combines conventional and advanced treatments in parallel lines. Sci. Total Environ. 461–462, 618–626. https://doi.org/10.1016/j.scitotenv.2013.05.026.

Fujii, Y., Harada, K.H., Haraguchi, K., Koizumi, A., 2017. Long-term Trends in Dietary Intake of Perfluoroalkyl Carboxylic Acids in Relation to Their Serum Concentration in Two Regions in Japan from 1979 to 2011. Chemosphere. https://doi.org/10.1016/j.chemosphere.2017.02.073.

Garcia-Costa, A.L., Savall, A., Zazo, J.A., Casas, J.A., Groenen Serrano, K., 2020. On the role of the cathode for the electro-oxidation of perfluorooctanoic acid. Catalysts 10, 902. https://doi.org/10.3390/catal10080902.

Gebbink, W.A., van Leeuwen, S.P.J., 2020. Environmental contamination and human exposure to PFASs near a fluorochemical production plant: review of historic and current PFOA and GenX contamination in The Netherlands. Environ. Int. 137, 105583. https://doi.org/10.1016/j.envint.2020.105583.

Ghanbari, F., Moradi, M., 2017. Application of peroxymonosulfate and its activation methods for degradation of environmental organic pollutants: Review. Chem. Eng. J. 310, 41–62. https://doi.org/10.1016/j.cej.2016.10.064.

Gobelius, L., Hedlund, J., Dürig, W., Tröger, R., Lilja, K., Wiberg, K., Ahrens, L., 2018. Per- and polyfluoroalkyl substances in Swedish groundwater and surface water: implications for environmental quality standards and drinking water guidelines. Environ. Sci. Technol. 52, 4340–4349. https://doi.org/10.1021/acs.est.7b05718.

Goeden, H.M., Greene, C.W., Jacobus, J.A., 2019. A transgenerational toxicokinetic model and its use in derivation of Minnesota PFOA water guidance. J. Expo. Sci. Environ. Epidemiol. 29, 183–195. https://doi.org/10.1038/s41370-018-0110-5.

Gomez-Ruiz, B., Diban, N., Urtiaga, A., 2019. Comparison of microcrystalline and ultrananocrystalline boron doped diamond anodes: influence on perfluorooctanoic acid electrolysis. Separ. Purif. Technol. 208, 169–177. https://doi.org/10.1016/j.seppur.2018.03.044.

Gomis, M.I., Vestergren, R., Borg, D., Cousins, I.T., 2018. Comparing the toxic potency in vivo of long-chain perfluoroalkyl acids and fluorinated alternatives. Environ. Int. 113, 1–9. https://doi.org/10.1016/j.envint.2018.01.011.

Grandjean, P., Timmermann, C.A.G., Kruse, M., Nielsen, F., Vinholt, P.J., Boding, L., Heilmann, C., Molbak, K., 2020. Severity of COVID-19 at elevated exposure to perfluorinated alkylates. MedRxiv Prepr. Serv. Heal. Sci. https://doi.org/10.1101/2020.10.22.20217562.

Guo, R., Sim, W.-J., Lee, E.-S., Lee, J.-H., Oh, J.-E., 2010. Evaluation of the fate of perfluoroalkyl compounds in wastewater treatment plants. Water Res. 44, 3476–3486. https://doi.org/10.1016/j.watres.2010.03.028.

Heydebreck, F., Tang, J., Xie, Z., Ebinghaus, R., 2015. Alternative and legacy perfluoroalkyl substances: differences between European and Chinese river/estuary systems. Environ. Sci. Technol. https://doi.org/10.1021/acs.est.5b01648.

Hongkachok, C., Boontanon, S.K., Boontanon, N., Fujii, S., Tanaka, S., Suzuki, Y., 2018. Levels of perfluorinated compounds (PFCs) in groundwater around improper municipal and industrial waste disposal sites in Thailand and health risk assessment. Water Sci. Technol. 2017, 457–466. https://doi.org/10.2166/wst.2018.168.

Hopkins, Z.R., Sun, M., DeWitt, J.C., Knappe, D.R.U., 2018. Recently detected drinking water contaminants: GenX and other per- and polyfluoroalkyl ether acids. J. Am. Water Works Assoc. 110, 13–28. https://doi.org/10.1002/awwa.1073.

Hu, X.C., Andrews, D.Q., Lindstrom, A.B., Bruton, T.A., Schaider, L.A., Grandjean, P., Lohmann, R., Carignan, C.C., Blum, A., Balan, S.A., Higgins, C.P., Sunderland, E.M., 2016. Detection of poly- and perfluoroalkyl substances (PFASs) in U.S. drinking water linked to industrial sites, military fire training areas, and wastewater treatment plants. Environ. Sci. Technol. Lett. 3, 344–350. https://doi.org/10.1021/acs.estlett.6b00260.

Kannan, K., Newsted, J., Halbrook, R.S., Giesy, J.P., 2004. Perfluorooctanesulfonate and related fluorinated hydrocarbons in mink and river otters from the United States. Environ. Sci. Technol. 38, 1264. https://doi.org/10.1021/es0354061, 1264.

Lang, J.R., Allred, B.M., Field, J.A., Levis, J.W., Barlaz, M.A., 2017. National estimate of per- and polyfluoroalkyl substance (PFAS) release to U.S. municipal landfill leachate. Environ. Sci. Technol. 51, 2197–2205. https://doi.org/10.1021/acs.est.6b05005.

Lin, H., Niu, J., Ding, S., Zhang, L., 2012. Electrochemical degradation of perfluorooctanoic acid (PFOA) by Ti/SnO_2–Sb, Ti/SnO_2–Sb/PbO_2 and Ti/SnO_2–Sb/MnO_2 anodes. Water Res. 46, 2281–2289. https://doi.org/10.1016/j.watres.2012.01.053.

Liu, Z., Sartori, A.F., Buijnsters, J.G., 2021. Role of sp^2 carbon in non-enzymatic electrochemical sensing of glucose using boron-doped diamond electrodes. Electrochem. Commun. 130, 107096. https://doi.org/10.1016/j.elecom.2021.107096.

Macpherson, J.V., 2015. A practical guide to using boron doped diamond in electrochemical research. Phys. Chem. Chem. Phys. 17, 2935–2949. https://doi.org/10.1039/C4CP04022H.

McGuire, M.E., Schaefer, C., Richards, T., Backe, W.J., Field, J.A., Houtz, E., Sedlak, D.L., Guelfo, J.L., Wunsch, A., Higgins, C.P., 2014. Evidence of remediation-induced alteration of subsurface poly- and perfluoroalkyl substance distribution at a former firefighter training area. Environ. Sci. Technol. 48, 6644–6652. https://doi.org/10.1021/es5006187.

Merlen, A., Buijnsters, J., Pardanaud, C., 2017. A guide to and review of the use of multiwavelength Raman spectroscopy for characterizing defective aromatic carbon solids: from graphene to amorphous carbons. Coatings 7, 153. https://doi.org/10.3390/coatings7100153.

Moreira, F.C., Boaventura, R.A.R., Brillas, E., Vilar, V.J.P., 2017. Electrochemical advanced oxidation processes: a review on their application to synthetic and real wastewaters. Appl. Catal., B 202, 217–261. https://doi.org/10.1016/j.apcatb.2016.08.037.

Mortet, V., Živcová, Z.V., Taylor, A., Davydová, M., Frank, O., Hubík, P., Lorincik, J., Aleshin, M., 2019. Determination of atomic boron concentration in heavily boron-doped diamond by Raman spectroscopy. Diam. Relat. Mater. 93, 54–58. https://doi.org/10.1016/j.diamond.2019.01.028.

Mullin, L., Katz, D.R., Riddell, N., Plumb, R., Burgess, J.A., Yeung, L.W.Y., Jogsten, I.E., 2019. Analysis of hexafluoropropylene oxide-dimer acid (HFPO-DA) by liquid chromatography-mass spectrometry (LC-MS): review of current approaches and environmental levels. TrAC Trends Anal. Chem. (Reference Ed.). https://doi.org/10.1016/j.trac.2019.05.015.

Niu, J., Li, Y., Shang, E., Xu, Z., Liu, J., 2016. Electrochemical oxidation of perfluorinated compounds in water. Chemosphere 146, 526–538. https://doi.org/10.1016/j.chemosphere.2015.11.115.

Niu, J., Lin, H., Gong, C., Sun, X., 2013. Theoretical and experimental insights into the electrochemical mineralization mechanism of perfluorooctanoic acid. Environ. Sci. Technol. 47, 14341–14349. https://doi.org/10.1021/es402987t.

Niu, J., Lin, H., Xu, J., Wu, H., Li, Y., 2012. Electrochemical mineralization of perfluorocarboxylic acids (PFCAs) by Ce-doped modified porous nanocrystalline PbO_2 film electrode. Environ. Sci. Technol. 46, 10191–10198. https://doi.org/10.1021/es302148z.

Ochiai, T., Iizuka, Y., Nakata, K., Murakami, T., Tryk, D.A., Fujishima, A., Koide, Y., Morito, Y., 2011. Efficient electrochemical decomposition of perfluorocarboxylic acids by the use of a boron-doped diamond electrode. Diam. Relat. Mater. 20, 64–67. https://doi.org/10.1016/j.diamond.2010.12.008.

Olsen, G.W., Burris, J.M., Ehresman, D.J., Froelich, J.W., Seacat, A.M., Butenhoff, J.L., Zobel, L.R., 2007. Half-life of serum elimination of perfluorooctanesulfonate, perfluorohexanesulfonate, and perfluorooctanoate in retired fluorochemical production workers. Environ. Health Perspect. https://doi.org/10.1289/ehp.10009.

Parsons, J.R., Sáez, M., Dolfing, J., de Voogt, P., 2008. Biodegradation of perfluorinated compounds. Reviews of Environmental Contamination and Toxicology, pp. 53–71. https://doi.org/10.1007/978-0-387-78444-1_2.

Pica, N.E., Funkhouser, J., Yin, Y., Zhang, Z., Ceres, D.M., Tong, T., Blotevogel, J., 2019. Electrochemical oxidation of hexafluoropropylene oxide dimer acid (GenX): mechanistic insights and efficient treatment train with nanofiltration. Environ. Sci. Technol. 53, 12602–12609. https://doi.org/10.1021/acs.est.9b03171.

Pico, Y., Blasco, C., Farré, M., Barceló, D., 2012. Occurrence of perfluorinated compounds in water and sediment of L'Albufera natural park (València, Spain). Environ. Sci. Pollut. Res. 19, 946–957. https://doi.org/10.1007/s11356-011-0560-y.

Pierpaoli, M., Szopińska, M., Wilk, B.K., Sobaszek, M., Łuczkiewicz, A., Bogdanowicz, R., Fudala-Książek, S., 2021. Electrochemical oxidation of PFOA and PFOS in landfill leachates at low and highly boron-doped diamond electrodes. J. Hazard Mater. 403, 123606. https://doi.org/10.1016/j.jhazmat.2020.123606.

Prevedouros, K., Cousins, I.T., Buck, R.C., Korzeniowski, S.H., 2006. Sources, fate and transport of perfluorocarboxylates. Environ. Sci. Technol. 40, 32–44. https://doi.org/10.1021/es0512475.

Rahman, M.F., Peldszus, S., Anderson, W.B., 2014. Behaviour and fate of perfluoroalkyl and polyfluoroalkyl substances (PFASs) in drinking water treatment: a review. Water Res. 50, 318–340. https://doi.org/10.1016/j.watres.2013.10.045.

RIVM, 2019. Verspreiding van GenX-stoffen in het milieu. RIVM, Rapp.

Sartori, A.F., Orlando, S., Bellucci, A., Trucchi, D.M., Abrahami, S., Boehme, T., Hantschel, T., Vandervorst, W., Buijnsters, J.G., 2018. Laser-induced periodic surface structures (LIPSS) on heavily boron-doped diamond for electrode applications. ACS Appl. Mater. Interfaces 10, 43236–43251. https://doi.org/10.1021/acsami.8b15951.

Schaefer, C.E., Andaya, C., Burant, A., Condee, C.W., Urtiaga, A., Strathmann, T.J., Higgins, C.P., 2017. Electrochemical treatment of perfluorooctanoic acid and perfluorooctane sulfonate: insights into mechanisms and application to groundwater treatment. Chem. Eng. J. 317, 424–432. https://doi.org/10.1016/j.cej.2017.02.107.

Schwenke, K.U., Spiehl, D., Krauße, M., Riedler, L., Ruppenthal, A., Villforth, K., Meckel, T., Biesalski, M., Rupprecht, D., Schwall, G., 2019. Analysis of free chlorine in aqueous solution at very low concentration with lateral flow tests. Sci. Rep. 9, 17212. https://doi.org/10.1038/s41598-019-53687-0.

Soriano, Á., Gorri, D., Urtiaga, A., 2017. Efficient treatment of perfluorohexanoic acid by nanofiltration followed by electrochemical degradation of the NF concentrate. Water Res. 112, 147–156. https://doi.org/10.1016/j.watres.2017.01.043.

Springer Berlin Heidelberg, 2013. Stockholm convention on persistent organic pollutants (POPs). In: Encyclopedia of Corporate Social Responsibility. Springer Berlin Heidelberg, Berlin, Heidelberg, p. 2336. https://doi.org/10.1007/978-3-642-28036-8_101506, 2336.

Stoiber, T., Evans, S., Naidenko, O.V., 2020. Disposal of products and materials containing per- and polyfluoroalkyl substances (PFAS): a cyclical problem. Chemosphere 260, 127659. https://doi.org/10.1016/j.chemosphere.2020.127659.

Sun, M., Arevalo, E., Strynar, M., Lindstrom, A., Richardson, M., Kearns, B., Pickett, A., Smith, C., Knappe, D.R.U., 2016. Legacy and emerging perfluoroalkyl substances are important drinking water contaminants in the Cape Fear river watershed of North Carolina. Environ. Sci. Technol. Lett. https://doi.org/10.1021/acs.estlett.6b00398.

The Organisation for Economic Co-operation and Development (OECD), 2018. Toward a New Comprehensive Global Database of Per- and Polyfluoroalkyl Substances (PFASs): Summary Report on Updating the OECD 2007 List of Per- and Polyfluoroalkyl Substances (PFASs), Series on Risk Management.

Trautmann, A.M., Schell, H., Schmidt, K.R., Mangold, K.-M., Tiehm, A., 2015. Electrochemical degradation of perfluoroalkyl and polyfluoroalkyl substances (PFASs) in groundwater. Water Sci. Technol. 71, 1569–1575. https://doi.org/10.2166/wst.2015.143.

Urtiaga, A., Fernández-González, C., Gómez-Lavín, S., Ortiz, I., 2015. Kinetics of the electrochemical mineralization of perfluorooctanoic acid on ultrananocrystalline boron doped conductive diamond electrodes. Chemosphere 129, 20–26. https://doi.org/10.1016/j.chemosphere.2014.05.090.

Vecitis, C.D., Park, H., Cheng, J., Mader, B.T., Hoffmann, M.R., 2009. Treatment technologies for aqueous perfluorooctanesulfonate (PFOS) and perfluorooctanoate (PFOA). Front. Environ. Sci. Eng. China 3, 129–151. https://doi.org/10.1007/s11783-009-0022-7.

Wang, G., Wang, X., Xing, Z., Lu, J., Chang, Q., Tong, Y., 2019. Occurrence and distribution of perfluorooctane sulfonate and perfluorooctanoic acid in three major rivers of Xinjiang, China. Environ. Sci. Pollut. Res. 26, 28062–28070. https://doi.org/10.1007/s11356-019-05770-2.

Wang, L., Lu, J., Li, L., Wang, Y., Huang, Q., 2020. Effects of chloride on electrochemical degradation of perfluorooctanesulfonate by Magnéli phase Ti_4O_7 and boron doped diamond anodes. Water Res. 170, 115254. https://doi.org/10.1016/j.watres.2019.115254.

Zhang, K., Huang, J., Yu, G., Zhang, Q., Deng, S., Wang, B., 2013. Destruction of perfluorooctane sulfonate (PFOS) and perfluorooctanoic acid (PFOA) by ball milling. Environ. Sci. Technol. 47, 6471–6477. https://doi.org/10.1021/es400346n.

Zhuang, Y., Wang, X., Zhang, L., Kou, Z., Shi, B., 2020. Confinement Fenton-like degradation of perfluorooctanoic acid by a three dimensional metal-free catalyst derived from waste. Appl. Catal., B 275, 119101. https://doi.org/10.1016/j.apcatb.2020.119101.

Zhuo, Q., Deng, S., Yang, B., Huang, J., Wang, B., Zhang, T., Yu, G., 2012. Degradation of perfluorinated compounds on a boron-doped diamond electrode. Electrochim. Acta 77, 17–22. https://doi.org/10.1016/j.electacta.2012.04.145.

Zhuo, Q., Deng, S., Yang, B., Huang, J., Yu, G., 2011. Efficient electrochemical oxidation of perfluorooctanoate using a Ti/SnO_2-Sb-Bi anode. Environ. Sci. Technol. 45, 2973–2979. https://doi.org/10.1021/es1024542.